Experimental Investigation of the Effects of Fluid Viscosity on Electrical Submersible Pumps Performance

W. Monte Verde[1]*, E. Kindermann[2], J. L. Biazussi[1], V. Estevam[1], B. P. Foresti[3], and A. C. Bannwart[1]

[1]Center for Petroleum Studies, University of Campinas
[2]School of Mechanical Engineering, University of Campinas
[3]Petrobras

Summary

Electrical submersible pumps (ESPs) are an important artificial lift method used in oil production. ESPs can provide high production flow rate, are flexible, and can be installed in highly deviated wells, subsea deepwater wells, or on the seabed. ESP performance is generally characterized by manufacturers using only water as fluid. However, oil properties are very different from water and significantly alter the pump's performance. Operating ESPs with viscous fluids leads to degraded pump performance. Therefore, knowing the ESP's performance when pumping viscous fluid is essential to properly design the production system. In this work, we present an experimental study of ESP performance operating with viscous flow. A total of six ESP models were tested, operating at four different rotational speeds and 11 viscosities, resulting in a comprehensive database of more than 5,800 operating conditions. This database contributes to the literature given the lack of available data. We also perform a phenomenological analysis on the influence of operational parameters, such as viscosity, rotational speed, specific speed, and rotational Reynolds number. The database and analyses performed are central for future models predicting the viscous performance of ESPs. The results from our investigation and tests showed that the increase in viscosity causes (1) a reduction in the head and (2) an increase in drive power, resulting in (3) a sharp decrease in efficiency. However, increasing rotational speed tends to mitigate this performance degradation. Efficiency and flow rate correction factors are virtually independent of the flow rate within the recommended operating region. This is not true for the head correction factor, which is not constant. The pump geometry seems to influence its performance as ESPs with higher specific speed are less impaired by viscous effects. The database obtained in the present work is available in the data repository of the University of Campinas, at the address presented by Monte Verde et al. (2022).

Introduction

Throughout the history of petroleum exploration, centrifugal pumps have proved to be effective for oil production. In fact, one of the most traditional artificial lifting methods is the electrical submersible pumping system, the main component of which is a multistage centrifugal pump known as ESP. This turbomachinery supplies energy to the oil and thus increases the flow rate in naturally flowing wells and even enables the production in pumping wells. Zhu et al. (2019) highlight the importance of the ESP system and classify this artificial lifting method as the second most used worldwide and the first when it comes to production volume.

The application of ESP systems in the petroleum industry is a result, among other factors, of the constant innovations that have made this technology more flexible. At the start of the 20th century, the development of submersible electric motors enabled the emergence of the first ESP system, which was initially used in the exploration of onshore oil fields (Takacs 2009). With the advance of oil production in deepwater fields, the ESP system started being used in dry wellhead installations. Then, in the mid-1980s, after the establishment of offshore wells in the Campos Basin in Brazil, the demand for an alternative method for gas lift boosted the development of an ESP system suitable for wells with wet completion (Silva et al. 2000).

In the last decades, the innovations related to the ESP system have focused on removing the equipment from inside the producing well. Such modification sought to mitigate one of the main disadvantages of the ESP system in wet completion: high workover cost to replace the system. In this sense, one of the most relevant solutions developed was the pumping module, known as MoBo, which consists of an ESP system outside the production well and housed in a dummy well downstream the wet Christmas tree (Colodette et al. 2008). Another recent technology, which eliminates the need for a dummy well, is the ESP skid or mudline ESP. This system consists of an ESP mounted within capsules in a skid, which is then positioned on the seabed (Costa et al. 2013; Rodrigues et al. 2005; Monte Verde et al. 2021).

Regarding future perspectives, the use of ESPs for oil production points to a promising scenario. The exploration of fields that are farther from the coast, in deep waters, is costly and renders additional technical difficulties to maintain large inhabited platforms responsible for the oil production. In this context, the concept of subsea to shore arises (i.e., a technique for producing directly to the continent with the use of subsea boosting systems installed on the seabed). This very concept also has another relevant application—the development of satellite wells far from the stationary production unit. For both applications, several solutions for submarine boosting have been discussed in the literature, and some make use of centrifugal pumps that are comparable to the ESP skid, which may possibly be driven by permanent magnet motors operating at high speeds (Shakirov et al. 2018).

However, these technologies cause ESPs to operate at lower intake pressure and temperature. The lower pressure in the ESP intake may promote the release of light oil fractions, causing a more viscous liquid phase. When this condition is associated with the lower temperature of the seabed, the liquid phase becomes even more viscous. The high viscosity at the ESP intake located on or near the seabed will have a direct effect on its operation. The performance degradation due to viscous effects is even more severe in these pumps when compared to conventional ESP systems.

In the scenario of oil production using ESPs, pump performance degradation due to oil viscosity is a top issue. In addition to layouts that take the pump out of the well, heavy oil production is another application that degrades ESP performance. Furthermore, when high

*Corresponding author; email: wmv@unicamp.br

Original SPE manuscript received for review 25 May 2022. Revised manuscript received for review 3 July 2022. Paper (SPE 210603) peer approved 6 July 2022.

water fraction is produced with oil, intense shear can produce emulsions that have an effective viscosity greater than the viscosity of pure oil. Despite this performance limitation, ESPs are still attractive as they can provide high production flow rates, being the only possible artificial lift method to develop some heavy oil offshore fields.

The ESP viscous performance must be predicted when designing the system. However, the manufacturers usually provide the performance of ESPs working with single-phase water flow. From these reference curves, correction factors are applied or energy losses are subtracted, providing the performance prediction for more viscous fluids. When the ESP sizing is done properly and considers the viscous effects, it is possible to overcome the trouble of performance degradation and operate at the designed flow rate. Furthermore, ensuring ESP system's use within the operational envelope has important economic implications due to the high costs involved in failures, breakdowns, and downtime. The properly sized equipment, operating with greater efficiency, is essential to reducing the carbon emission per barrel of oil produced. Therefore, the need to investigate the effects of fluid viscosity on ESPs performance is evident.

Literature Review. Daugherty (1926) and Ippen (1946) conducted pioneering studies on the centrifugal pumps' performance working with viscous fluids. The investigation developed by Ippen (1946) involved four centrifugal pump models, different rotational speeds, and three types of oil, which resulted in more than 220 tests. This was the first systematic study of centrifugal pump performance with viscosity increase under controlled laboratory flow conditions. In this work, the author defines fundamental concepts about viscous losses in centrifugal pumps.

Stepanoff (1949) later conducted experimental tests and proposed empirical correlations to obtain the viscous correction factors and then predict the pump's performance. Although limited to the design point, the correlations proposed by Stepanoff (1949) are still widely used today, as well as the hypothesis of constant specific speed, regardless of the viscosity of the fluid being pumped.

Hydraulic Institute Standards (1955) proposed a standardized method for estimating the centrifugal pump performance in viscous flow service when the water performance curve is given. This methodology was based on an extensive database of volute centrifugal pumps from 1 to 8 in. of flange diameter and kinematic viscosity ranging from 4 to 3,300 cSt. The correction factors were obtained through graphs depending on the operating parameters for water service and viscosity. This method was digitalized by Hole (1994) and Turzo et al. (2000) to generate the easy-use calculation formulations.

ANSI/HI 9.6.7 (2021) is the current version of this method, which provides empirical correlations for the correction factors. Certainly, this is one of the most used methods in the industry for predicting the viscous performance of conventional centrifugal pumps.

Gülich (1999a, 1999b, 2008) carried out relevant studies on the topic, providing empirical and semiempirical models to predict pump performance under viscous medium. The comprehensive study of viscous losses in rotors and volutes is one of the most relevant in the literature.

Although ESPs are essentially multistage centrifugal pumps, their geometry is quite different from volute centrifugal pumps. In general, the aforementioned studies were based on volute, radial, large diameter, and single-stage pumps. The ESPs used in oil production have radial, mixed, or axial geometry; stator instead of volute; small diameters; and multiple stages. Amaral et al. (2009) conducted one of the first experimental studies applied to ESPs. In the study, the authors compared the measured ESP performance to those predicted by traditional models, such as the Hydraulic Institute Standards (1955), revealing high deviations. Monte Verde (2016) also conducted an experimental investigation and extended the performance comparisons to the Stepanoff (1957), Gülich (2008), and ANSI-HI models, showing even greater deviations for predicting the performance of a three-stage ESP.

The high deviations in the performance prediction caused by the application of models developed for volute pumps to ESPs boosted studies dedicated to the oil industry. **Table 1** shows the experimental studies to determine the viscous performance of ESPs.

Author	Content	Pump	Fluid
Amaral et al. (2009)	Experimental study on the performance of ESP operating with ultraviscous oil	GN7000–3 stg	1 to 1020 mPa·s
Solano (2009)	Viscous effects on the performance of ESPs	DN1750–7 stg	70 to 1160 mPa·s
Barrios et al. (2012)	ESP technology maturation: Subsea boosting system with high gas/oil ratio and viscous fluids	WJE1000–32 stg	1 to 2800 mPa·s
Monte Verde (2016)	Performance modeling of ESP pumps performance operating with gas-viscous liquid mixtures	GN5200–3 stg	1 to 1069 mPa·s
Zhang (2017)	Experiments, computational fluid dynamics (CFD) simulation, and modeling of ESP performance under viscous fluid flow conditions	TE2700–14 stg	37 to 107 mPa·s
Banjar (2018)	Experiments, CFD simulation, and modeling of oil viscosity and emulsion effects on ESP performance	DN1750–7 stg	56 to 220 mPa·s
Bulgarelli et al. (2021a)	Experimental investigation on the performance of ESP operating with unstable water/oil emulsions	P100L–8 stg	1 to 300 mPa·s
Porcel et al. (2022)	Experimental study on the performance of ESP operating with ultraviscous oil	HC20000–10 stg	8 to 4170 mPa·s

Table 1—Experimental studies of ESPs operating with viscous fluid available in the literature.

Experimental studies are limited in the literature as they are costly and require large laboratory structures. Other approaches, such as analytical modeling (Sun and Prado 2006; Biazussi 2014; Morrison et al. 2018; Zhu et al. 2019) and numerical simulations (Zhu et al. 2016; Ofuchi et al. 2017, 2020; Patil and Morrison 2019), have also been developed.

Recently, more works have focused on oil/water emulsion flow in ESPs as the strong shearing effect creates a fine dispersion of oil and water mixture, which in turn significantly increases the apparent viscosity (Bulgarelli et al. 2021a, 2021b, 2022; Perissinotto et al. 2019a, 2019b, 2020).

In general, the main limitation observed in the literature is the lack of open experimental data on the ESP performance pumping viscous fluids, making databases rare in the open literature. This limitation hinders advances in the area as experimental data are essential for the development of performance prediction models and correlations, whether they are empirical, semiempirical, or numerical. Therefore,

further studies that provide open and reliable databases are essential, thus enabling a phenomenological analysis of the operational parameters' influence on viscous performance.

The objective of this work is to present head, flow rate, and efficiency correction factors, providing an open, broad, and reliable performance database of six ESP models under controlled laboratory conditions operating at four rotational speeds and 11 different viscosities, resulting in 181 characteristics curves and more than 5800 operational points. This database is relevant regarding the studies in **Table 1**. This work also aims to provide a phenomenological analysis of the influence of operational parameters, such as viscosity, rotational speed, rotational Reynolds number, and, pioneering, the specific speed. Such analysis provides useful insights that are the basis of performance prediction models, which will be presented in future works.

Experimental Methodology

This section presents the experimental methodology used to obtain ESP performance when pumping viscous fluids.

Experimental Facility. The ESP performance tests were conducted in the Experimental Laboratory of Petroleum–LABPETRO, at the University of Campinas–UNICAMP. The ESP assembly and the supply equipment that compose the loop are shown in **Figs. 1 and 2,** respectively. The schematic diagram of the ESP loop test is shown in **Fig. 3.**

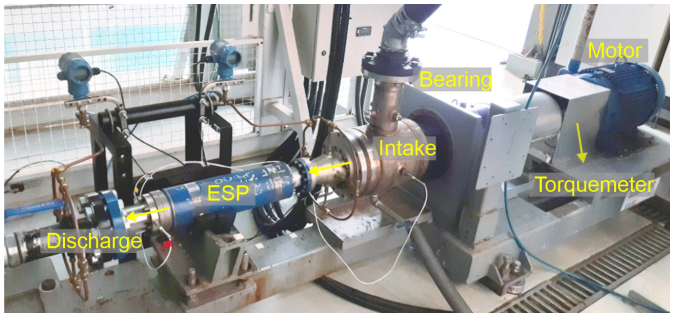

Fig. 1—ESP assembly.

Fig. 2—Supply equipment.

The loop test was designed to operate with water or viscous fluid. Water is stored in Tank 1 and its circulation is carried out by a centrifugal booster pump, with a flow rate limit of 70 m^3/h. In the viscous fluid operation, the storage is carried out in Tank 2. In this case, the circuit is supplied by a positive displacement helical booster pump that can provide up to 100 m^3/h at a viscosity of 1000 mPa·s. The booster pumps are used to overcome pressure drops upstream of the ESP, providing positive intake pressure. Both booster pumps are driven by remotely controlled variable speed drivers (VSD1 and VSD2), which allow the adjustment of the ESP intake pressure during the tests.

After being pumped by the booster, the working fluid flows through the closed temperature control system, which is composed of a thermo-chiller, a thermo-regulator, and a shell-and-tube heat exchanger. The thermo-regulator receives the temperature setpoint from the supervisory control system and supplies water at constant temperature. The water process then flows through the heat exchanger and heats or cools the working fluid.

The electropneumatic globe valve (V1) controls the working fluid flow through the heat exchanger and is therefore another parameter for temperature control. This system allows heating or cooling of the working fluid between 10 and 50°C.

Precise thermal control is essential in viscous tests as the fluid viscosity is adjusted through temperature. Thus, it is possible to obtain a wide range of viscosities with the same fluid by controlling its temperature at the ESP intake.

Before the ESP intake, the fluid mass flow rate is measured by a Coriolis meter, series DS300, manufactured by Emerson Micro Motion®. This sensor has a maximum range of 190 500 kg/h and an accuracy of 0.15%. The fluid is then pumped by the ESP, flows

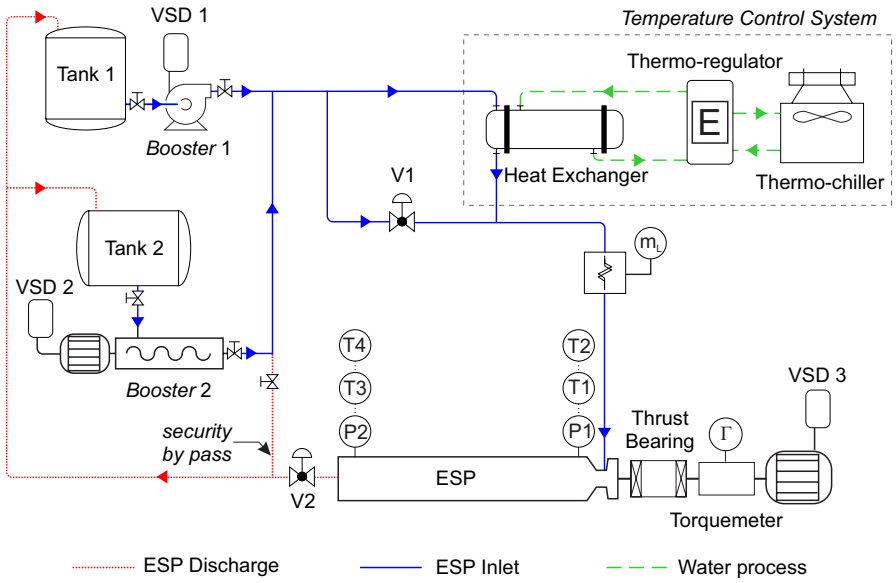

Fig. 3—Schematic diagram of the ESP loop test.

through the electropneumatic globe valve (V2), and returns to the storage tank (Tank 1 or Tank 2), depending on the working fluid used. Valve V2 is used to provide backpressure to the ESP discharge for flow rate control in the test circuit.

The ESP is driven by a three-phase induction electric motor of 50 hp controlled by VSD3. The ESP motor assembly is positioned horizontally. Between the motor and the ESP intake, a thrust bearing and a rotary torquemeter are installed. The torquemeter is from the T21WN series, manufactured by HBM®, with an accuracy of 0.2% and a maximum range of 200 N·m. The shaft torque is the mechanical parameter used to calculate the driving power or brake horsepower (BHP). The rotational speed is measured with a photo tachometer, series MDT-2238A, manufactured by Minipa®, with an accuracy of 0.05%.

The pressure and temperature are measured at the ESP intake and discharge. Capacitive transducers, series 2051, manufactured by Rosemount®, are used to measure the gauge pressure. The pressure sensors have an accuracy of 0.075%.

The temperature is measured with a resistance temperature detector, type PT100, 4 wires, and 1/10 DIN, with standard accuracy. A two-sensor redundancy is used, both in the ESP intake and discharge. The intake temperature is used as a reference in fluid viscosity control, while the temperature in the discharge helps estimate the heating of the pumped fluid.

All instruments are connected to a data acquisition system, manufactured by National Instruments®, connected to a LabView® code, which monitors, controls, and stores data.

ESPs. For the ESP selection, some assumptions were considered. (1) Restrictions regarding the operational limits of the experimental facility. (2) Restrictions regarding the number of ESP stages. We opted to test ESPs in three stages, which is enough to minimize the inlet effects without causing excessive heating of the working fluid. One can consider that the viscosity is practically constant through the pump and can thus assume an average ESP performance. (3) This premise aims to compose a set of equipment that covers the largest possible range of specific speeds.

Thus, six models of three-stage ESPs were selected. These ESPs are from 538 and 675 series, manufactured by Baker Hughes®, as shown in **Table 2.**

ESP	Series	Number of Stages	Impeller Diameter (mm)
P37	538	3	108
P47	538	3	108
P62	538	3	108
P100	538	3	108
HC10000	675	3	134
HC12500	675	3	134

Table 2—Set of tested ESPs.

Working Fluids. Experimental tests were performed using three working fluids—tap water, double-distilled glycerin, and solution of water in double-distilled glycerin. For simplicity, the double-distilled glycerin is simply called “glycerin” and the solution of water in double-distilled glycerin is called “diluted glycerin.”

Glycerin was chosen due to its easy handling, low environmental risk, and wide viscosity variation from temperature changes. This allows the ESPs to operate at different viscosities, with the same fluid, by controlling the temperature.

The glycerin was used for the medium- and high-viscosity matrix, while diluted glycerin was used for low viscosities. Water tests are useful as a performance benchmark and to validate the proper operation of the experimental facility, ESPs, measurement instruments, and operational procedure. The properties of glycerin and diluted glycerin were measured, while standard properties were considered for tap water.

The rheological analyses of glycerin and diluted glycerin were performed using a rotational rheometer (Thermoscientific Co., model Haake Mars III). The fluid behavior was evaluated under shear stress scanning in the range of 25 to 500 seconds^{-1}, in the operational limits of 15 and 50°C. These analyses indicated that glycerin and the diluted glycerin present Newtonian behavior in these temperature limits. Fluid viscosity as a function of temperature was measured by setting the shear rate at 100 seconds^{-1} and varying the temperature at a decreasing rate of 0.4 °C/min, from 50 to 15°C.

The densities of glycerin and diluted glycerin were measured using a vibrating tube densimeter (Anton Paar, model DMA4500), with temperature control of the measuring cell by a Peltier element.

Fig. 4 shows the glycerin and diluted glycerin properties as a function of temperature. Considering the temperature limits of 15 to 50°C, it is possible to obtain a range of glycerin viscosities from 1800 to 120 mPa·s (1440 to 100 mm^2/s), respectively. For diluted glycerin, this range is 176 to 23 mPa·s (144 to 19 mm^2/s). The density is represented by the dashed lines.

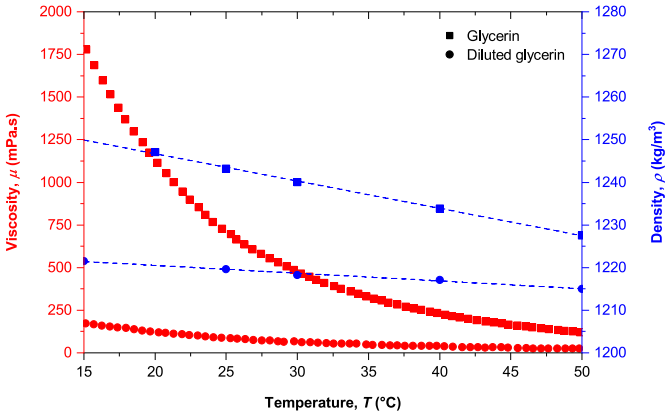

Fig. 4—Glycerin and diluted glycerin properties as a function of temperature.

The specific heat of glycerin, used to analyze the pumped fluid heating, was characterized using a differential scanning calorimeter (TA Instruments, model Q2000). The measurement procedure consists of filling the sample holder with 10 mg of glycerin, which is then hermetically sealed and a heating rate of 20 °C/min is applied from 15 to 50°C while maintaining a nitrogen atmosphere. The specific heat presents a very small increase as a function of the temperature. This variation is within the uncertainty range of the calorimeter and, for application in this work, the specific heat can be assumed constant and equal to 2.355 kJ/kg·K.

Test Matrix. Standard tests with water are essential as viscous degradation is calculated based on this reference. Temperature does not significantly affect water properties and during the tests it was around 30°C. Thus, water viscosity was considered around 1 mPa·s. The first tests were thus carried out with water for each ESP, as shown in **Table 3.**

ESP	Temperature (°C)	Viscosity (mPa·s)	Rotational Speed (rev/min)
P37	~30	~1	
P47			3,500
P62			3,000
P100			2,400
HC10000			1,800
HC12500			

Table 3—Water test matrix.

Then, ESP performance tests were carried out with up to 11 different viscosities. Glycerin provided the medium to high viscosity range (i.e., 128 to 1273 mPa·s or 104 to 1020 mm^2/s). Diluted glycerin, on the other hand, provided the matrix with low viscosity, between 24 and 88 mPa·s (20 to 72 mm^2/s). These values encompass the viscosity range of light to heavy oils.

Viscous tests were performed at three different rotational speeds. For the 538 series ESPs (P37, P47, P62, and P100), the tests were performed at 2,400, 3,000, and 3,500 rev/min. The ESPs of the 675 series (HC10000 and HC12500), given the limitation of available power, were tested at 1,800, 2,400, and 3,000 rev/min.

Table 4 presents the test matrix with glycerin. There are eight viscosities: 128, 226, 330, 474, 655, 847, 1036, and 1273 mPa·s. (104, 183, 266, 382, 527, 680, 831, and 1020 mm^2/s). Briefly, testing a total of six ESP models, operating at three rotational speeds and eight viscosities, results in 144 viscous performance curves.

ESP	Temperature (°C)	Dynamic Viscosity (mPa·s)	Kinematic Viscosity (mm^2/s)	Rotational Speed (rev/min)
	18.8	1273	1020	
	21.0	1036	831	
P37	23.2	847	680	
P47	26.1	655	527	3,500
P62	30.0	474	382	3,000
P100	34.8	330	266	2,400
	40.0	226	183	
	47.0	128	104	
	18.8	1273	1020	
	21.0	1036	831	
	23.2	847	680	
HC10000	26.1	655	527	3,000
HC12500	30.0	474	382	2,400
	34.8	330	266	1,800
	40.0	226	183	
	47.0	128	104	

Table 4—Glycerin test matrix.

Table 5 shows the lower viscosity matrix performed with diluted glycerin. There are three viscosities: 24, 50, and 88 mPa·s (20, 41, and 72 mm^2/s).

ESP	Temperature (°C)	Dynamic Viscosity (mPa·s)	Kinematic Viscosity (mm^2/s)	Rotational Speed (rev/min)
P37	25	88	72	3,500, 3,000, 2,400
	35	50	41	
	50	24	20	3,500, 2,400
P47	25	88	72	3,500, 3,000, 2,400
	35	50	41	
	50	24	20	
P62	25	88	72	3,500, 3,000, 2,400
	35	50	41	
	50	24	20	3,000, 2,400
P100	25	88	72	3,000, 2,400
	35	50	41	
	50	24	20	–
HC10000	25	88	72	1,800
	35	50	41	2,400, 1,800
	50	24	20	
HC12500	25	88	72	1,800
	35	50	41	
	50	24	20	

Table 5—Diluted glycerin test matrix.

For each viscosity, the tests were also carried out in three rotational speeds. However, due to the experimental limitations, some curves were removed from the matrix. The effective experimental matrix of six ESPs with the diluted glycerin provided 37 curves.

Therefore, the complete viscous matrix provides 181 curves, with viscosity ranging from 24 to 1273 mPa·s (20 to 1020 mm^2/s), composing a database of 181 best efficiency points (BEPs) and more than 5,800 operational points.

Experimental Procedure. The experimental procedure aims to measure the performance parameters required to obtain the characteristic curves (i.e., $H \times Q$, BHP $\times Q$, and $\eta \times Q$). For each curve, the fluid viscosity (and hence the temperature) must be kept constant at the ESP intake. This proves difficult since the flow rate ranges from the open flow to shutoff condition during the test. The ESP efficiency and,

consequently, the system entropy generation also varies along the curve. Thus, it is necessary to adjust the water process temperature and Valve V1 opening at each collected point.

The limits of ±0.1°C around the temperature setpoint were established as acceptable for constant temperature assumption.

The test procedure is based on *API RP 11S2* (1997). Once the inlet temperature setpoint has been reached and is stable, the test starts from the open flow condition. Data acquisition is performed over an interval of 30 seconds, with a sampling rate of 1 kHz, resulting in 30000 samples per measurement. The acquisition software calculates and stores the arithmetic mean of this sample. Then, Valve V2 is closed until the next flow rate point. When steady state is reached again, data acquisition is performed. This procedure is repeated until the flow reaches the shutoff condition (i.e., zero flow rate).

For each curve, between 20 and 50 points are acquired, a number higher than the five points recommended by the *API RP 11S2* standard.

When pumping water, the test procedure is similar, but the rigorous control of temperature is not required as in the viscous tests.

Results

This section includes the results of ESP performance in viscous service. For convenience, trends and analyses are presented only for a single ESP when the results are valid for the other models. The database with the performance of all models is available in the data repository of the University of Campinas, at the address presented by Monte Verde et al. (2022).

ESP Performance Pumping Water. The total useful power P_h transmitted by the pump to the fluid can be calculated using the energy conservation. Considering steady-state, isentropic, and incompressible flow, the useful power per ESP stage is:

$$P_h = \rho g H Q, \tag{1}$$

where ρ is the density, g is the gravity acceleration, Q is the volumetric flow rate, and H is the total stage head. H is the sum of the pressure, velocity, and geodetic head.

Usually, velocity and geodetic terms are negligible and stage H is essentially equal to the change in pressure head:

$$H = \frac{1}{N}\left(\frac{P_2 - P_1}{\rho g}\right), \tag{2}$$

where P is the pressure, N is the ESP number of stages, and the sub-indexes 1 and 2 represent the pump intake and discharge, respectively.

Note that Eq. 1 provides only useful energy (or hydraulic power) as the heat exchange with the external environment and internal fluid heating, due to entropy generation, are disregarded.

The power required to drive each stage of the ESP is the BHP:

$$\mathrm{BHP} = \frac{1}{N}(\omega \Gamma), \tag{3}$$

where ω is the rotational speed and Γ the shaft torque.

The pump efficiency (η) is defined as:

$$\eta = \frac{P_h}{\mathrm{BHP}}. \tag{4}$$

The dimensionless pump performance can also be used. The dimensionless parameters are flow rate (ϕ), head (ψ), power coefficients (Π), and rotational Reynolds number (Re_ω).

$$\psi = \frac{gH}{\omega^2 D^2}, \tag{5}$$

$$\phi = \frac{Q}{\omega D^3}, \tag{6}$$

$$\Pi = \frac{\mathrm{BHP}}{\rho \omega^3 D^5}, \tag{7}$$

$$\mathrm{Re}_\omega = \frac{\rho \omega D^2}{\mu}, \tag{8}$$

where D is the impeller diameter and μ is the dynamic viscosity. Note that Eqs. 5 and 7 yield the coefficients per stage.

Fig. 5 shows the dimensionless performance of ESP P47, pumping water at different speeds. The other ESP models have the same behaviors and trends, so they are not shown in the manuscript.

One can notice the curves overlapping in different speeds and that the efficiency, head, and power coefficients are approximately unique functions of the flow rate coefficient [i.e., $\psi \approx f_1(\phi)$, $\Pi \approx f_2(\phi)$, and $\eta \approx f_3(\phi)$]. These results indicate fully turbulent flow, where the Re_ω has a constant effect and does not influence the performance parameters.

Dimensionless performance curves were fitted by nonlinear regressions (dashed lines) using fifth-order polynomials. For head coefficient, all ESPs have regressions with coefficient of determination (R^2) greater than 0.9973. For dimensionless power, the smallest R^2 is 0.9672, referring to model P62. For efficiency, all regressions present R^2 greater than 0.9880, also for ESP P62.

These results are in line with the similarity laws applied to turbomachinery, so the analysis indicates that the experimental procedure, instrumentation, and ESPs work properly.

Accurate definition of the BEP for ESPs pumping water is essential as this data defines its optimum operating range and specific speed. In addition, water BEPs are used as a reference for correlations that provide viscous correction factors.

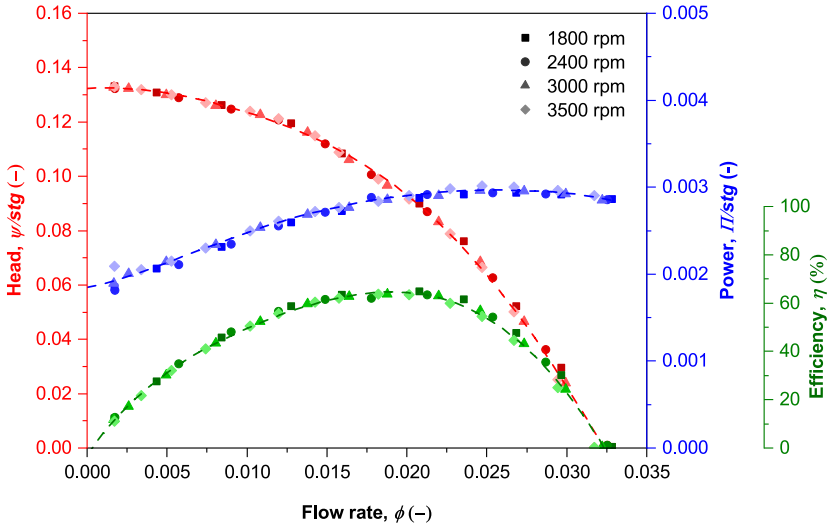

Fig. 5—ESP P47 dimensionless performance with water.

The BEPs were obtained from dimensionless ESP performance. Based on the fitted regressions, the maximum point for the $\eta\, x\, \phi$ curve is calculated to obtain the flow rate coefficient (ϕ_{BEP}) at the BEP. Then, this value is applied to the other curves, and the head (ψ_{BEP}) and power (Π_{BEP}) coefficients at the BEP are obtained. The dimensional parameters for different rotational speeds are obtained by applying Eqs. 5 through 7. Using this procedure, ϕ_{BEP} and ψ_{BEP} are the same for all rotational speeds. Thus, the specific speed (ω_s) defined for a single stage can be calculated by Eq. 9, yielding a constant value for each ESP model, regardless of the rotational speed.

$$\omega_S = \frac{\phi_{BEP}^{1/2}}{\psi_{BEP}^{3/4}} = \frac{\omega Q_{BEP}^{1/2}}{g H_{BEP}^{3/4}}. \quad (9)$$

Eq. 9 yields the dimensionless specific speed. However, it is common practice in the oil industry to use American units, resulting in a dimensional specific speed (N_S):

$$N_S = \frac{\omega Q_{BEP}^{1/2}}{H_{BEP}^{3/4}}, \quad (10)$$

where $[\omega]$ is revolutions per minute, $[Q_{BEP}]$ is gallons per minute, and $[H_{BEP}]$ is feet; and the conversion factor is $N_s = 2{,}733.7\ \omega_s$.

Fig. 6 shows the specific speed and the performance characteristics of the ESP models pumping water at 3,500 rev/min (presented in order of increasing N_s). The ESP set covers the range of $1{,}795 < N_s < 3{,}198$, $22.4 < Q_{BEP} < 83.8$ m^3/h, and $12.3 < H_{BEP} < 29.5$ m. According to the classification proposed by Chapallaz et al. (1992), this specific speed range indicates ESPs with mixed-flow impeller profiles.

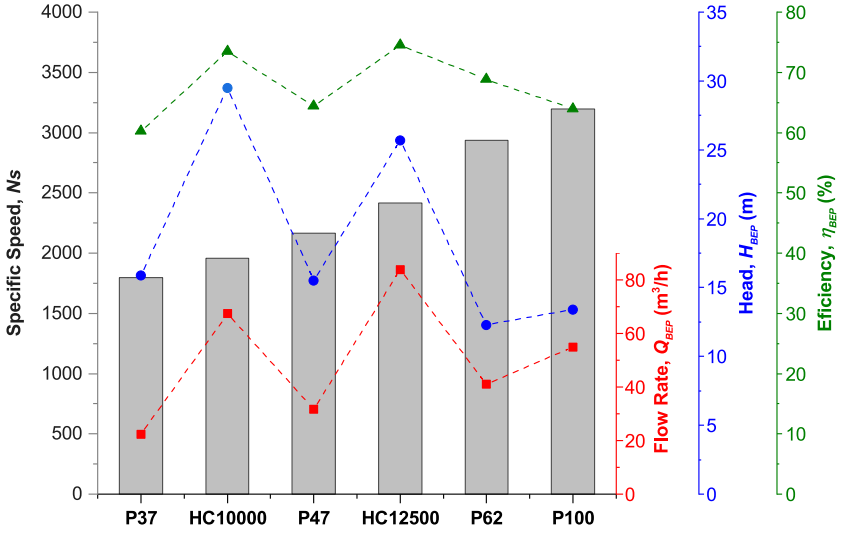

Fig. 6—ESP performance characteristics pumping water at 3,500 rev/min.

Fig. 7 shows the performance of ESP P47 pumping viscous fluid at 3,500 rev/min. This is a sample of viscous performance curve. Similar results were obtained for the other ESPs and speeds. The results for other ESP models are presented in the database available at Monte Verde et al. (2022).

Increasing fluid viscosity reduces the ESP ability to transfer angular momentum to the fluid, decreasing the head. Due to the increase in energy dissipation within the stages, the power consumed to drive the pump increases significantly. The decrease in head, associated

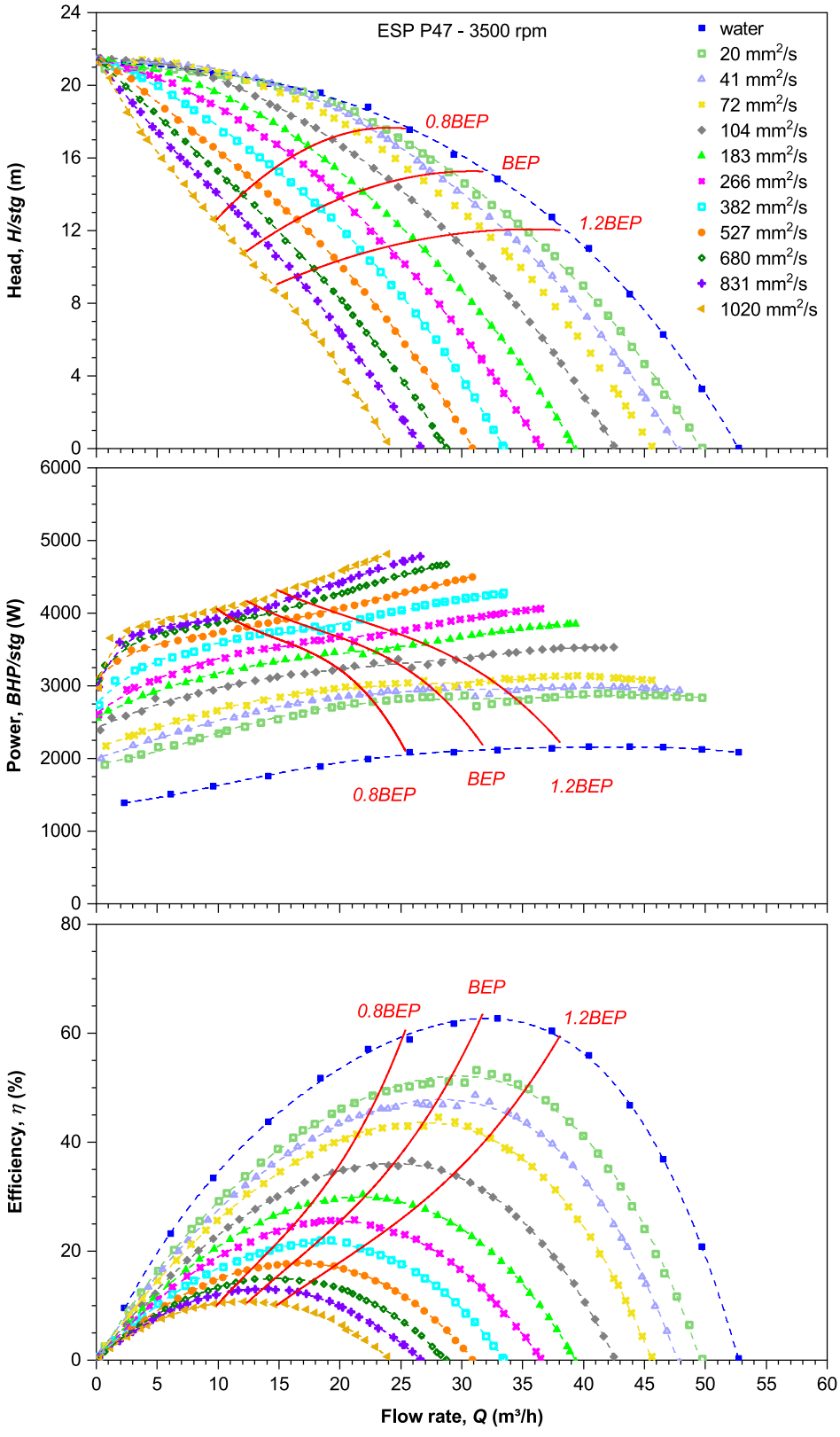

Fig. 7—ESP P47 performance pumping viscous fluid at 3,500 rev/min.

with the increase in BHP, results in a severe reduction in the ESP efficiency. The BEP flow rates and head decrease, shifting maximum efficiencies to the left of the curve as viscosity increases, are shown by the solid red lines in **Fig. 7**. The solid red lines also indicate the limits of 0.8 and 1.2 times the BEP flow rate.

For a constant speed, increasing viscosity decreases the ESP head and flow rate. However, at the shutoff condition, the head degradation is less significant and, in some cases, negligible. This changes the shape of the $H \times Q$ curve, making it "steeper." The ESP set, when pumping water, has flat or rising curves and tends to change into a steep curve as the viscosity increases. This means that the pressure gain increases suddenly with the flow rate reduction, when compared to other curve shapes. Some authors, such as Gülich (2008) and Stepanoff (1957), generalize that the shutoff head does not depend on fluid viscosity.

For the same flow rate, some points show a slightly higher viscous head than in water service. This occurs at low flow rates, close to shutoff, with the lowest viscosities of the test matrix, mainly for P47, HC10000, and HC12500. Similar behavior was observed by Barrios et al. (2012) in a slip-vane ESP. Such behavior can be explained by the fact that a small increase in viscosity reduces volumetric losses, which is composed of leakage and recirculation losses. In addition, hydraulic losses have less influence at points close to the shutoff since the fluid velocity is lower (Gülich 2008).

At points with the above conditions, the viscous fluid can seal leakages and the reduction in volumetric loss may be sufficient to overcome the increase in hydraulic losses, resulting in a head increase. However, even with a higher viscous head, the efficiency of these points is always lower than with water. This hypothesis is consistent because, in the low flow rate region, volumetric losses are dominant, while hydraulic losses become more significant at higher flow rates. According to Gülich (2008), the decrease in volumetric losses with increasing viscosity is important but less relevant than predicted considering the viscosity in the pump suction. Shear stress is high at these pump mechanical clearances, resulting in heating and local reduction in fluid viscosity.

As viscosity increases, the BHP curves move upward, approximately parallel to the water curve. The ESP set has typical behavior of mixed-flow pumps (i.e., the BHP increases continuously as a function of the flow rate until it reaches a maximum point after the BEP). Then, there is a mild decrease in required power, close to the open flow. However, with increasing viscosity, the typical behavior reported with water is modified. The BHP curves tend to increase monotonically (i.e., the consumed power increases as a function of the flow rate).

For higher viscosities, the operating conditions close to the shutoff show a smaller increase in BHP compared to other points. This is due to the high fluid heating in this region, reducing viscosity, and, consequently, reducing BHP. With a small flow rate increase, heating decreases and the BHP curve presents a greater slope at the points close to the shutoff. Stepanoff (1957) and Gülich (2008) attribute the increase in power consumed almost entirely to the increase in disk losses in this region.

Despite the sharp decrease in efficiency as a function of viscosity, the $\eta \times Q$ curves maintain the same shape and trend. Though these curves get "flattened," they are well represented by low-order polynomials. This curve flattening hinders the determination of the BEP because there is a wide region around maximum point with a slope close to zero. It is therefore possible to easily vary 5% of the flow rate around the BEP without a significant change in efficiency.

Viscous Correction Factors. How the ESP performance is modified from service with water to operation with viscous fluid can be estimated by empirical methods. Usually, this approach uses viscous correction factors. These parameters yield the viscous performance (subscript vis) relative to the standard performance with water (subscript w). The correction factors for flow rate (C_Q), head (C_H), and efficiency (C_η) are defined as:

$$C_Q = \frac{Q_{\text{vis}}}{Q_w}, \tag{11}$$

$$C_H = \frac{H_{\text{vis}}}{H_w}, \tag{12}$$

$$C_\eta = \frac{\eta_{\text{vis}}}{\eta_w}. \tag{13}$$

The correction factors are calculated for homologous conditions on the viscous and water curves. It is commonly assumed that the BEP flow rate in water service is homologous to the BEP flow rate with viscous fluid. The ratio between these flow rates in viscous and water operation defines the flow rate correction factor ($C_{Q,\text{BEP}}$). The heads and efficiencies corresponding to these flow rates define the other correction factors.

In addition to the BEP, another four characteristic points are defined in this study: 120% of BEP flow rate, 80% of BEP flow rate, 60% of BEP flow rate, and maximum flow rate. For these points, the water reference is also the homologous point. For example, the head correction factor for 120% ($C_{H,1.2\text{BEP}}$) is defined as the viscous head ($H_{\text{vis},1.2\text{BEP}}$) relative to the flow rate of $1.2Q_{\text{vis,BEP}}$ and the water head ($H_{w,1.2\text{BEP}}$) relative to the flow rate of $1.2Q_{w,\text{BEP}}$.

Rotational Speed and Viscosity Effect on Correction Factors. **Fig. 8** shows the BEP correction factors for ESP P47 under different rotational speeds and viscosities. As expected, the correction factors decrease as the viscosity increases, evidencing the increase in the pump performance degradation. For 3,500 rev/min, when increasing the fluid viscosity from 20 to 1020 mm^2/s, the head correction factor decreases from 0.970 to 0.684. This is related to increased friction in the impeller channels, which increases hydraulic losses, reducing the useful head delivered to the fluid. For the same viscosities and speed, the flow rate correction factor decreases from 0.930 to 0.390. The reduction in head and flow, added to the increase in disk friction loss due to the increase in viscosity, leads to a sudden reduction in pump efficiency. At 3,500 rev/min and 1020 mm^2/s, the P47 efficiency is reduced to only 16.7% of water service efficiency.

For constant rotational speed and viscosity, we observed $C_H > C_Q > C_\eta$. This result indicates that the head is less influenced by viscous effects compared to flow rate and efficiency. On the other hand, efficiency is the most impaired parameter because it depends on the viscous head and flow rate.

The efficiency correction factor curve shows a downward slope tendency as the viscosity increases. Gülich (1999b) attributes this behavior to the local thermal effects. For higher viscosities, the heat generated by the viscous dissipations attenuates the expected disk friction losses for the fluid temperature at the pump inlet. Under these conditions, thermal effects reduce the increase in BHP, minimizing the reduction in efficiency.

Fig. 8 also shows the rotational speed effect on correction factors. For a constant viscosity, head, flow rate, and efficiency, correction factors increase as the speed grows. Therefore, the viscous performance degradation decreases as a function of speed. Stepanoff (1957) and Monte Verde (2016) provide similar findings in their studies. Understanding this behavior is nontrivial as, in a centrifugal pump, the

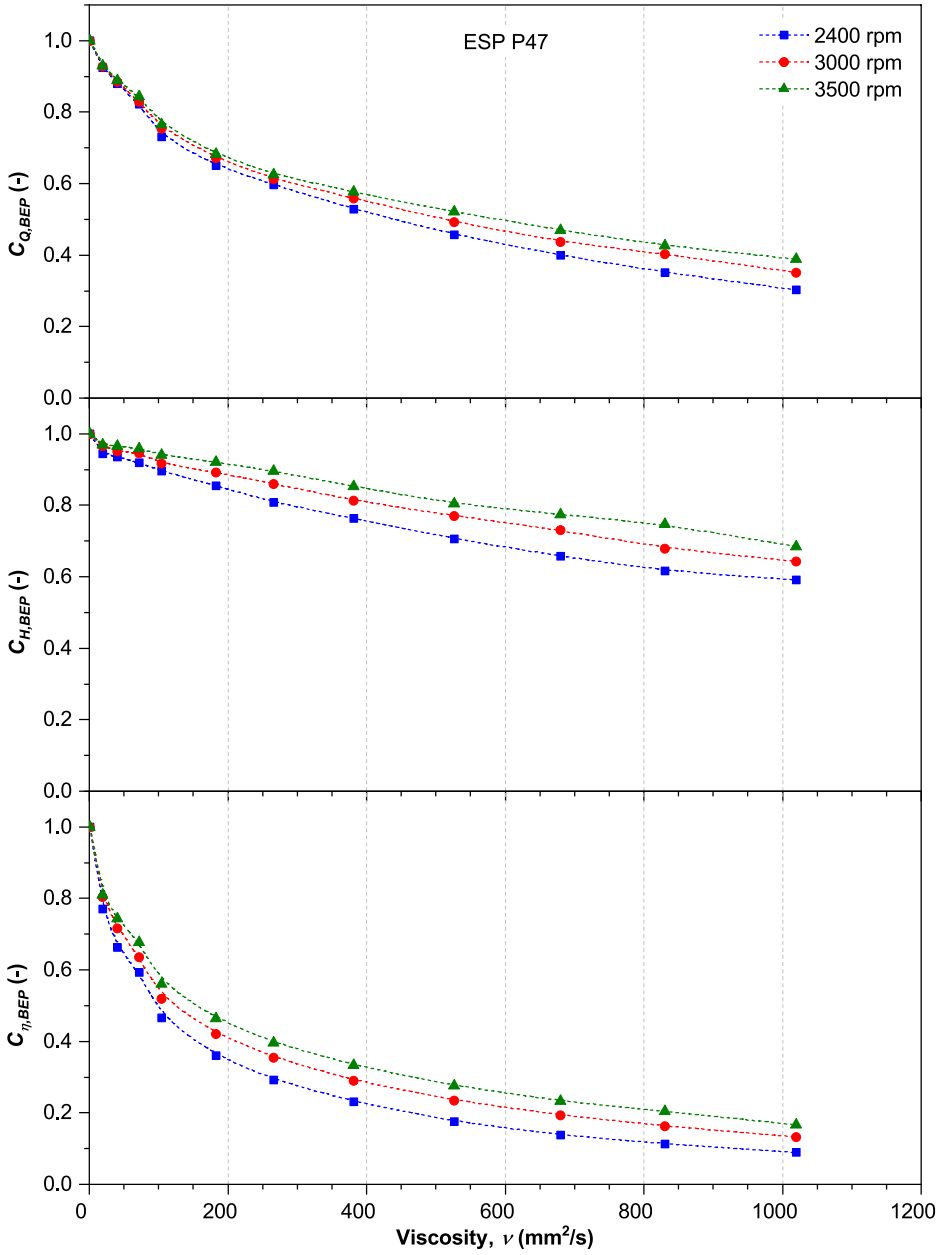

Fig. 8—Influence of viscosity and rotational speed on the BEP correction factors for ESP P47.

rotational speed influences the flow rate and head. A qualitative analysis can be proposed based on the two main energy losses that occur in the BEP—friction loss and disk friction loss.

Usually, the correlations proposed in the literature for the friction loss (h_f) are proportional to the friction factor (f) and the flow rate, such as: $h_f \propto fQ^2$. The friction factor is inversely proportional to the Reynolds number outside the region of complete turbulence. For the ESP operating at BEP, with constant viscosity, the higher the speed, the higher the flow rate and the Reynolds number and the lower the frictional factor. On the other hand, the friction loss is a quadratic function of the flow rate. In the combined effects of these two variables, the quadratic increase prevails, resulting in an increase in frictional loss as a function of rotational speed. However, the increase in friction loss tends to be less accentuated with the increase in flow rate and, consequently, the friction factor is smaller.

The increase in rotational speed also influences the pump head. For an inviscid flow, the head depends on the square of the rotational speed, as predicted by the affinity laws. In viscous service, this exponent tends to be higher.

When analyzing the head correction factors shown in **Fig. 8**, it is clear that the increase in head is proportionally higher than the increase in friction loss due to the higher rotational speed (i.e., the ratio h_f/H tends to be smaller because of the increase in rotational speed.

The power loss due to the disk friction (BHP_{disk}) is usually defined as a function of frictional factor (f), rotational speed (ω), and impeller diameter (D), such as: $BHP_{disk} \propto f\omega^3 D^5$ (Stepanoff 1957; Gülich 2008; Omar et al. 2017).

For an ESP operating with constant viscosity, the higher the rotational speed, the higher the flow rate and the Reynolds number and the lower the friction factor. On the other hand, disk power loss has a cubic dependency on the rotational speed. Thus, in the associated effect of these two variables, the cubic increase in speed prevails and the disk power loss increases as a function of rotational speed. However,

the increase in disk power loss tends to be less accentuated with the higher rotational speed, and consequently, the friction factor is smaller (i.e., the ratio BHP_{disk}/BHP tends to decrease with higher speed).

The influence of reducing the ratios h_f/H and BHP_{disk}/BHP given the increase in speed are combined in the efficiency, increasing the efficiency correction factor as shown in **Fig. 8**.

Effect of Operating Conditions on Correction Factors. **Fig. 9** shows the influence of operating conditions on correction factor for ESP P47 at 3,500 rev/min. The operating conditions are BEP flow rate; 0.6, 0.8, and 1.2 times BEP flow rate and maximum flow rate.

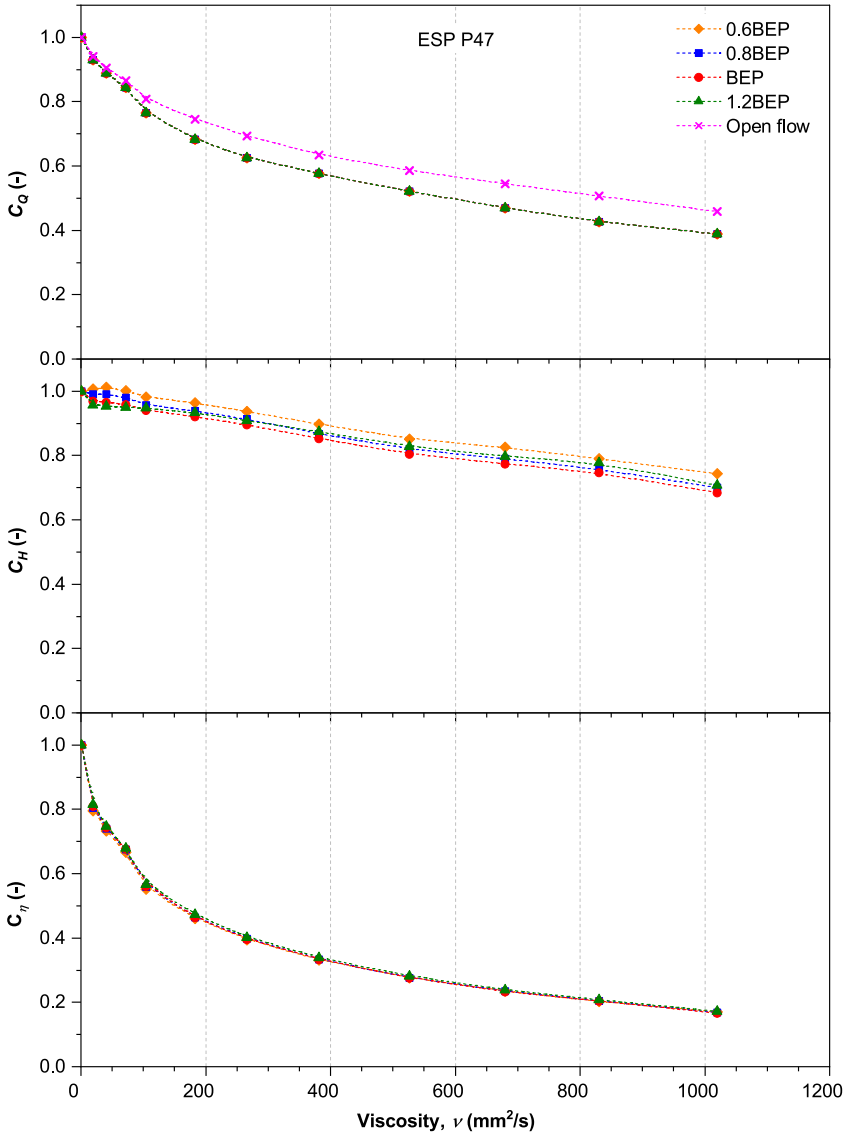

Fig. 9—Influence of operating conditions on correction factor for ESP P47 at 3,500 rev/min.

By definition $C_{Q,1.2BEP}$, $C_{Q,0.8BEP}$, and $C_{Q,0.6BEP}$ are equal to the BEP flow rate correction factor ($C_{Q,BEP}$), for example:

$$C_{Q,0.8BEP} = \frac{0.8Q_{vis,BEP}}{0.8Q_{w,BEP}} = \frac{Q_{vis,BEP}}{Q_{w,BEP}} = C_{Q,BEP}. \quad (14)$$

Therefore, any condition with operating flow rate multiple of BEP has a correction factor equal to the BEP. A different behavior is observed for the open flow condition, which has flow rate correction factor higher than the BEP.

Regarding the head correction factor, **Fig. 9** shows that head degradation depends on the operating condition, though these values are close. For a constant viscosity, we observed that $C_{H,0.6BEP} > C_{H,1.2BEP} > C_{H,0.8BEP} > C_{H,BEP}$. The head correction factor for open flow condition is not shown since the head is zero at this point.

Fig. 9 shows a relevant result regarding the efficiency correction factor. For a constant viscosity, the experimental results show that C_η does not depend on the operating condition multiples of BEP flow rate, that is: $C_{\eta,1.2BEP} \cong C_{\eta,0.8BEP} \cong C_{\eta,BEP}$.

The dependence of correction factors on the operating conditions showed in this section is useful for developing empirical models of viscous performance prediction. These results provide relevant insights into the hypothesis that can be assumed.

Rotational Reynolds Number Effect on Correction Factors. **Fig. 10** shows the BEP correction factors as a function of the rotational Reynolds number for ESP P47 at 2,400, 3,000, and 3,500 rev/min. Although the experimental conditions represent different rotational

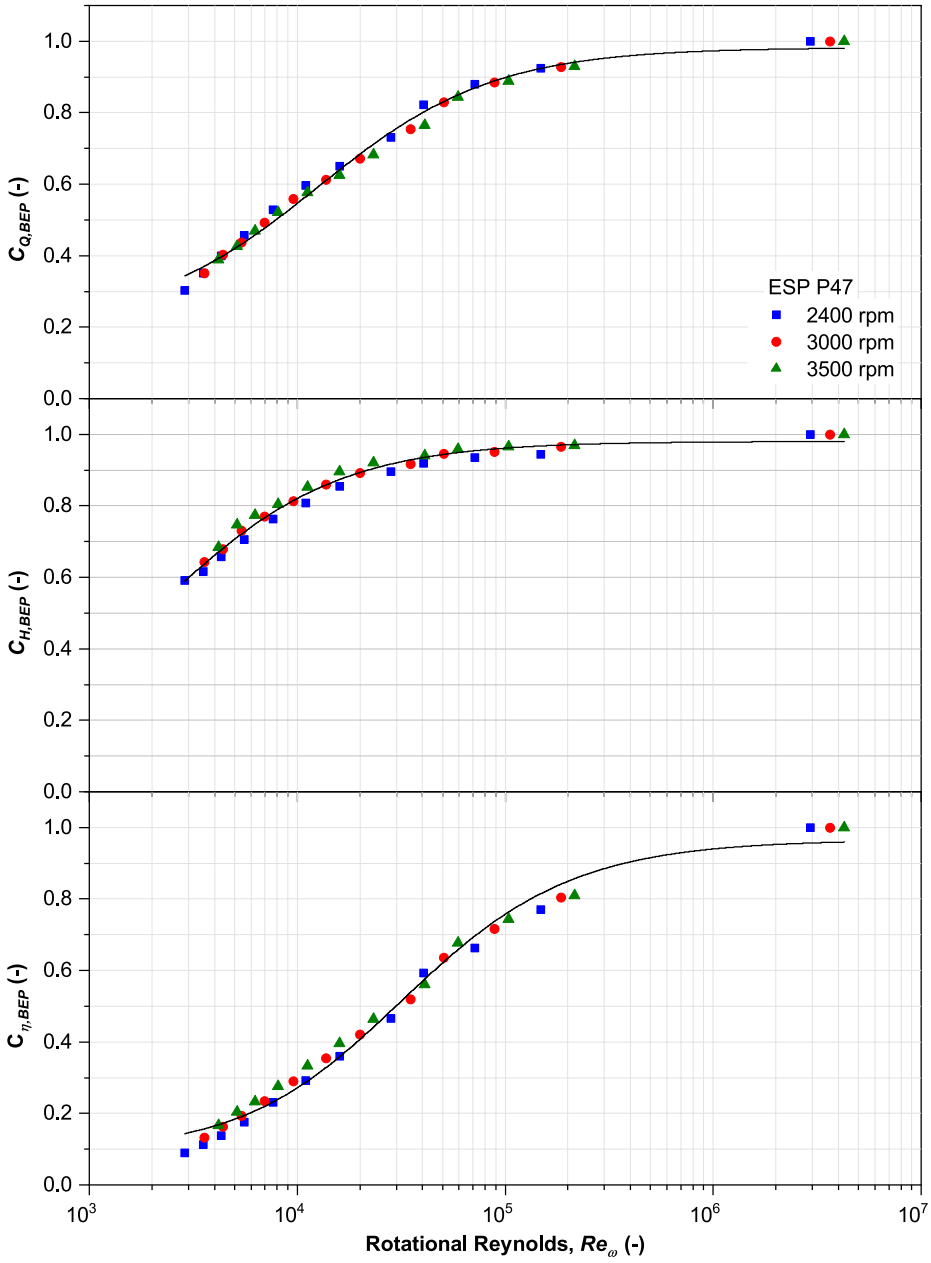

Fig. 10—Influence of Reynolds number on ESP P47 correction factor for different rotational speeds.

speeds and viscosities, the points merge into a single curve. The correction factors are approximately unique functions of the rotational Reynolds number, as fitted by the solid black lines [i.e., $C_{Q,\mathrm{BEP}} \approx f_1\left(\mathrm{Re}_\omega\right)$, $C_{H,\mathrm{BEP}} \approx f_2\left(\mathrm{Re}_\omega\right)$, and $C_{\eta,\mathrm{BEP}} \approx f_3\left(\mathrm{Re}_\omega\right)$].

For $\mathrm{Re}_\omega > 10^6$, the correction factors are approximately constant, unitary, and independent of the Reynolds number. Usually, the predominance of inertial forces is attributed to this region and turbulent flow is assumed. Within this region, no viscous corrections are needed.

On the other hand, for $\mathrm{Re}_\omega < 10^6$, the viscous effect is higher and, possibly, the laminar regime occurs. Determining the flow regime within the ESP stages is a hard task because the application of the rotational Reynolds number is not a consensus and there are no established transition limits that could be used to evaluate the flow regime.

Ofuchi et al. (2017) used the Reynolds number based on the hydraulic diameter of the channel to numerically evaluate the flow regime. For a 538 series ESP, operating between 1,800 and 3,500 rev/min, the flow was considered laminar for viscosities higher than 214 mm^2/s. Gülich (2008) states that depending on the size and speed of a conventional pump, the transition from turbulent to laminar flow occurs at about $\nu = 100\ \mathrm{mm}^2/\mathrm{s}$ and, for $\nu < 10\ \mathrm{mm}^2/\mathrm{s}$, the viscosity influence is negligible. On the other hand, Morrison et al. (2017, 2018) proposed transition limits to evaluate the flow regime based on the rotational Reynolds number. The laminar flow would occur for $\mathrm{Re}_\omega < 17,000$ and the turbulent flow for $\mathrm{Re}_\omega > 65,000$. The range between these values was defined as transition flow. This transition limits were proposed for $1,000 < N_s < 3,200$.

Therefore, this issue is still open and there is no established consensus in the literature about the flow regime boundaries within centrifugal pumps.

The correction factors dependence solely on the Reynolds number, as shown in **Fig. 10**, indicates an interesting way to propose empirical correlations for performance correction. For all ESP sets, the same trend was observed and the points nearly merge into a single curve. However, generalizations are quite difficult and dedicated correlations are needed for each ESP model.

Specific Speed Effect on Correction Factors. **Fig. 11** shows the specific speed effects on viscous performance of ESPs. These results show the BEP head, flow rate, and efficiency correction factors for all ESPs at 2,400 rev/min. The analysis of the other rotational speeds shows the same trends observed for 2,400 rev/min, so they are not presented. These results evidence the influence of the specific speed on the performance of ESPs from the same series (i.e., the same impeller diameter). For constant rotational speed and viscosity, it is clear that the viscous correction factors increase with higher specific speed for the ESPs from 538 series. Therefore, radial ESPs have greater performance degradation due to viscosity effects, while mixed-flow EPSs are less impaired. This trend is more evident in the flow rate and efficiency correction factors, as shown in **Fig. 12.**

Fig. 12 shows the flow rate and efficiency correction factors for the 538 series ESP working with different rotational Reynolds numbers. For high Re_ω, the viscous effects are negligible, the specific speed does not influence pump performance, and the correction factors are unitary. However, when Re_ω decreases, the ESP geometry becomes relevant. The curves for constant Re_ω slope slightly, indicating an increase in the correction factors for more axial ESPs.

The 675 series ESPs show the same behavior as the 538 series ESPs. However, when ESPs of different series are compared, we notice that the impeller diameter seems to influence the performance and the specific speed is not enough to define the performance dependence on the ESP geometry. For example, ESPs HC10000 and HC12500 have lower specific speed than P100; even so, these two 675 series ESPs show higher correction factors than the 538 series. Additional tests using other ESP series are needed to better evaluate the diameter influence on viscous performance for more conclusive analysis of this parameter.

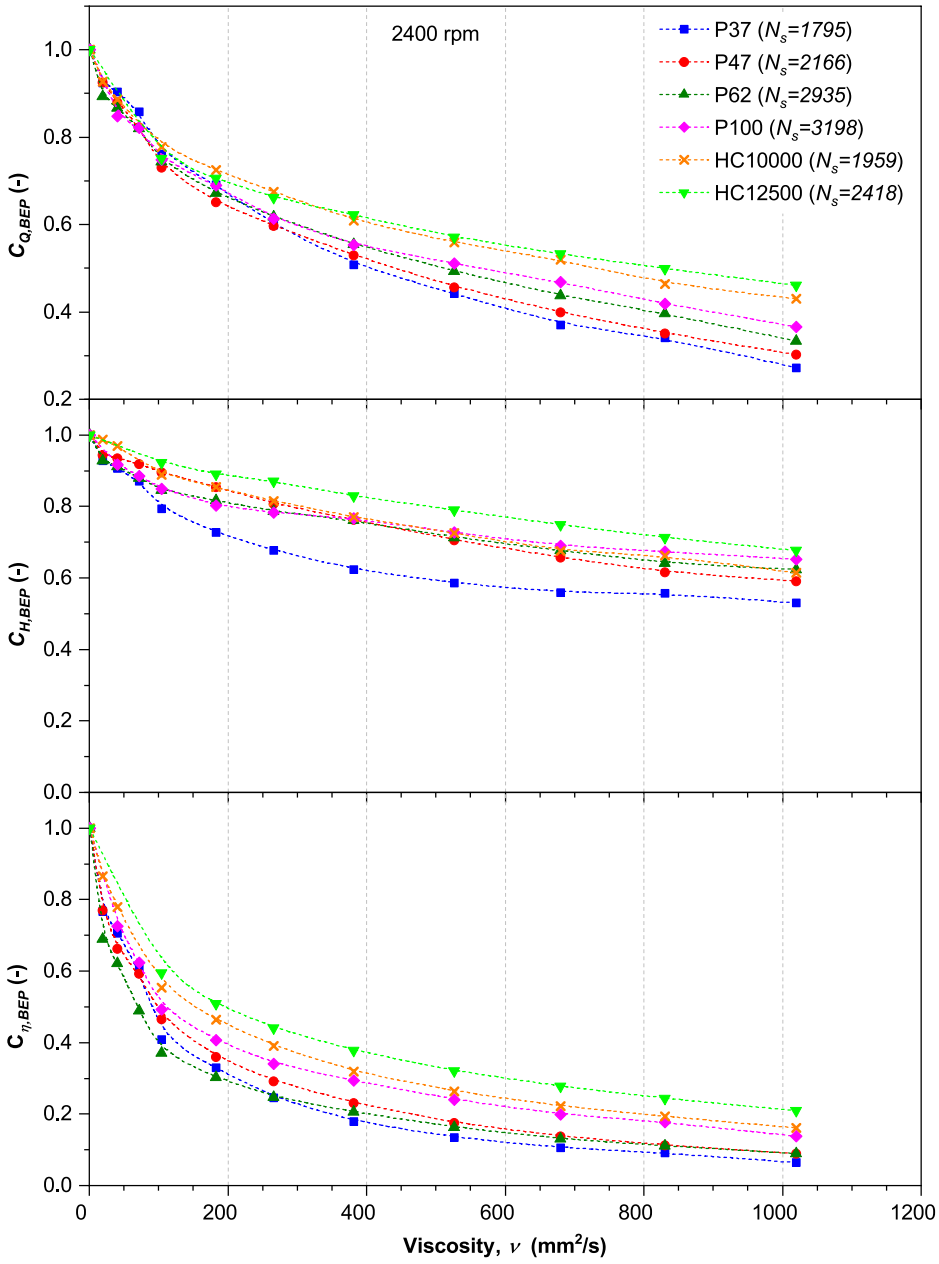

Fig. 11—Influence of specific speed on correction factor at 2,400 rev/min.

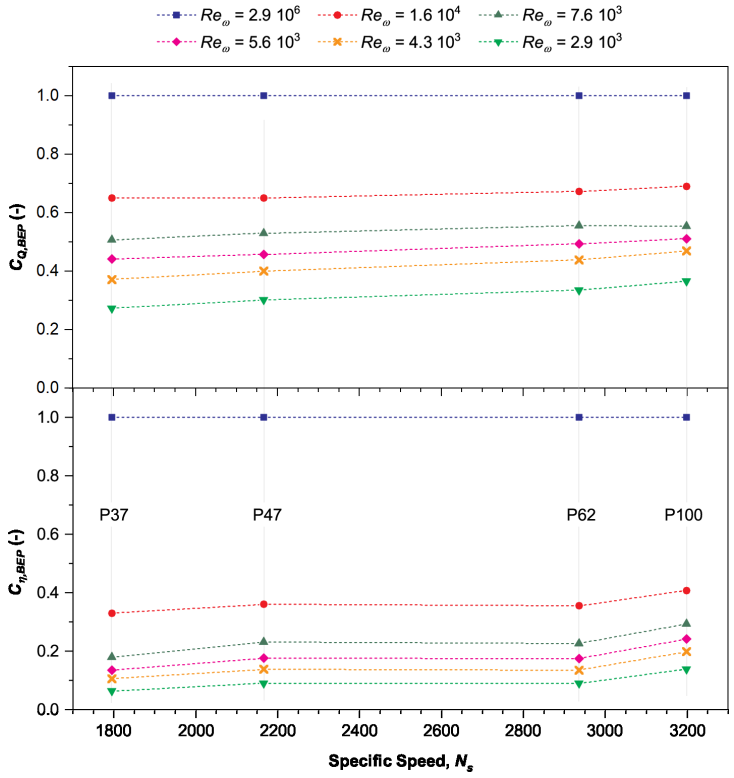

Fig. 12—Influence of specific speed on flow rate and efficiency correction factor for different Re_ω.

The influence of specific speed on viscous performance of centrifugal pumps is little discussed in the literature. Only a few studies propose correlations between energy losses and specific speed. Stepanoff (1957) and Gülich (2008) propose that leakage and disk friction losses tend to increase with the reduction of specific speed. However, these correlations are empirical and there is no mechanistic understanding of the physical phenomena.

As discussed in a previous section, the power loss due to the disk friction (BHP_{disk}) is a function of frictional factor. Stepanoff (1957) states that the friction factor depends on the clearance between the impeller and the pump casing, so the friction factor increases as the clearance thickness increases. Van Esch (1997) argues that disk friction depends on the flow regime and on the mechanical clearances thickness. According to this author, there are two separate boundary layers in pumps that have large-enough mechanical clearances. On the other hand, in pumps with small clearances, the boundary layers are merged. Thus, Van Esch (1997) presents four correlations for the friction factor as a function of these parameters that do not present the same tendency regarding the influence of mechanical clearance. On the other hand, Gülich (2008) proposes that the ratio between disk friction loss and BHP increases exponentially with the reduction of specific velocity. The author proposes numerous correlations for disk friction also as a function of radial clearance, flow regime, and additional impeller geometric characteristics. This underscores the different approaches from each author and it is not possible to establish a direct relationship between the increase in disk loss and the reduction in specific speed.

Understanding the reduction in performance degradation due to the increased diameter observed in the 675 series is neither a trivial nor intuitive task. According to the correlations proposed by Stepanoff (1957), Van Esch (1997), Biazussi (2014), Gülich (1999a, 1999b, 2008), and Omar et al. (2017), the disk friction loss increases sharply with a bigger diameter. However, it has been experimentally observed that increasing the diameter reduces viscous degradation. This suggests that the increased power loss due to the disk friction is compensated by the reduction of some other loss, so the net effect is the increase in efficiency.

One can therefore state that the experimental results are important because they indicate the influence of specific speed on ESP performance. However, such results are insufficient for a complete physical understanding of the phenomena. We highlight the importance of using ESPs from other series in the future test matrix to confirm the effects of diameter and specific rotation on viscous performance degradation.

Fluid Heating. Fig. 13 shows the fluid heating (ΔT) at BEP as a function of the specific speed, measured for 3,000 rev/min and viscosities of 183, 380, and 1020 mm^2/s. There is a tendency to increase the heating for more radial pumps (i.e., ESPs with lower specific speeds). This effect is intensified with higher viscosity. For example, for 183 mm^2/s, the heating is approximately constant and equal to 0.4°C for ESPs P37 and P100 (i.e., for $1{,}795 < N_s < 3{,}198$). For 1020 mm^2/s, the temperature increase is 1.1 and 0.6°C for models P37 and P100, respectively. We observed that the temperature increase is practically double for the more radial ESP compared to the more axial one.

We intuitively expected that the least efficient ESP have the highest temperature increase. However, other parameters also influence the pumped fluid heating. **Table 6** shows the performance parameters at BEP for 3,000 rev/min and 1020 mm^2/s (i.e., relative to the blue squares in **Fig. 13**). In this table, the ESPs are listed in ascending order of specific speed. These results show that efficiency does not necessarily decrease with the reduction of specific speed.

A simplified approach to estimating fluid temperature increase is obtained considering an integral energy balance, adiabatic flow, and assuming the idealization that all dissipated energy is converted into thermal energy. Thus, the temperature increase is:

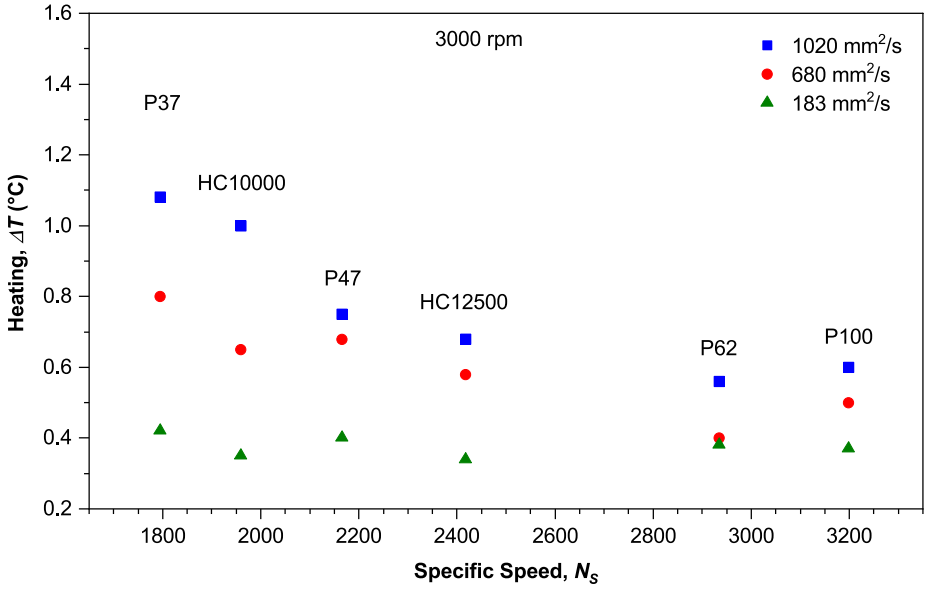

Fig. 13—Temperature increase at BEP for ESPs working at 3,000 rev/min and viscosities of 183, 680, and 1020 mm²/s.

ESP	Efficiency (%)	Heating (°C)	Head (H/stg)	Flow Rate (m^3/h)
P37	6.3	1.08	6.7	6.7
HC10000	16.0	1.00	14.2	28.4
P47	8.5	0.75	7.3	9.6
HC12500	18.8	0.68	16.1	28.3
P62	9.2	0.56	6.0	13.6
P100	12.5	0.60	6.8	19.3

Table 6—Performance characteristics at BEP for 3,000 rev/min and 1020 mm²/s.

$$\Delta T = \left(\frac{1}{\eta} - 1\right)\frac{\Delta P}{\rho c_P}, \tag{15}$$

where c_P is the fluid's specific heat.

Eq. 15 shows that the temperature increase also depends on the pressure increment, as does the efficiency. Mathematically, for the same efficiency and constant fluid properties, the greater the pressure gain, the greater the heating. This would explain the increase in heating with decrease of specific speed as N_S is inversely proportional to the pressure gain. However, for centrifugal pumps, the pressure gain, BHP, and efficiency are parameters that depend on flow rate, so the heating analysis must be carried out observing all available performance parameters.

The increase in heating as a function of ESP geometry can also be analyzed based on viscous losses. As discussed before, some authors propose that the power loss due to the disk friction is directly related to disk friction loss. According to Gülich (2008), the ratio between the power dissipated by disk friction and the hydraulic power is inversely proportional to the square of the specific speed. Therefore, the increase in energy dissipated due to disk friction is probably associated with greater heating of the fluid.

Fig. 14 shows the rotational effect on temperature increase for ESP P37. For constant rotational speed, we observed that heating increases significantly as a function of viscosity. This result is expected as the efficiency dramatically reduces as a function of viscosity, as shown in previous sections. However, an interesting result is observed when the influence of rotation speed on heating is analyzed. For a constant viscosity, we noticed that heating increases with higher speed.

This result corroborates previous discussions, which state that efficiency is not the only predominant factor for the heating analysis. As shown in **Fig. 8**, for a constant viscosity, increasing rotational speed tends to improve pump efficiency.

For example, for viscosity of 527 mm²/s in **Fig. 14**, the efficiencies of the ESP P37 are 8.1, 11.2, and 13.4%, for the rotational speed of 2,400, 3,000, and 3,500 rev/min, respectively. Efficiency improvement as a function of rotational speed is not enough to reduce heating. In addition to the efficiency improvement, the increase in rotational speed increases the pressure gain and flow rate. These results therefore suggest that the effect of pressure gain overlaps the increase in efficiency, causing an increase in heating as a function of rotational speed.

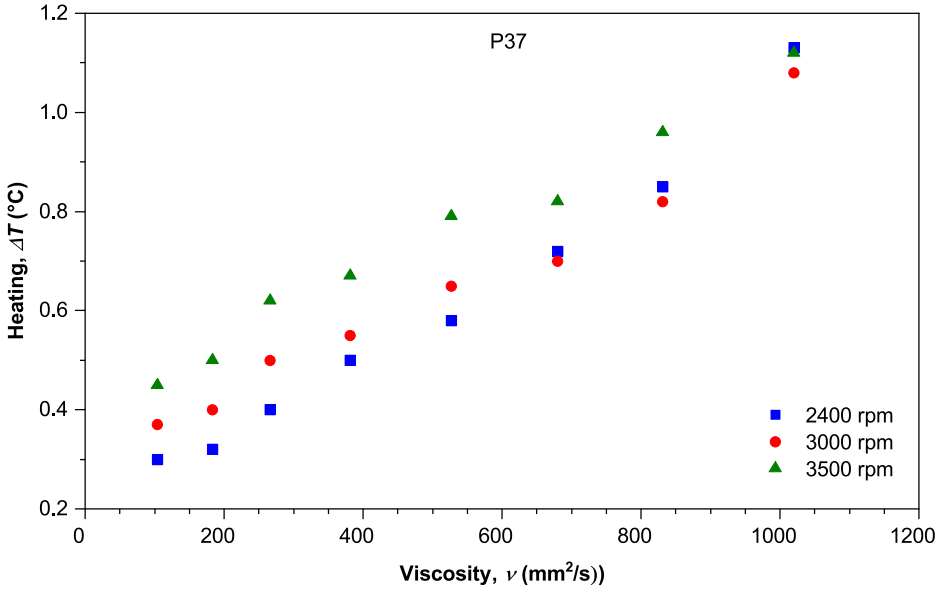

Fig. 14—Rotational speed effect on temperature increase for ESP P37.

Conclusions

This work provides a comprehensive and reliable performance database of six ESP models under controlled laboratory conditions, operating at four rotational speeds, 11 different viscosities, which resulted in 181 characteristics curves and more than 5800 operational points. From the experimental data, we performed phenomenological analyses of the influence of operational parameters, such as viscosity, rotational speed, specific speed, and rotational Reynolds number.

The following conclusions were obtained:

- These results contributed to the physical understanding of performance degradation and are the basis for performance prediction models and validation of numerical simulations.
- Increasing fluid viscosity reduced the ESP ability to transfer angular momentum to the fluid, decreasing the head. Due to the increase in energy dissipation within the stages, the power consumed to drive the pump increased significantly, while efficiency was greatly impaired.
- Correction factors decreased with higher viscosity, evidencing the increase in the pump performance degradation. However, performance degradation was mitigated with higher rotational speed.
- Any condition with operating flow rate multiple of BEP had flow rate correction factor equal to the BEP. The same was observed for the efficiency correction factor under the studied operating conditions. However, head correction factors depended on the operating condition, even though these values are close.
- For each ESP model, the correction factors were approximately unique functions of the rotational Reynolds number. Although the experimental conditions represent different rotational speeds and viscosities, the points merged into a single curve.
- For constant rotational speed and viscosity, we observed that the viscous correction factors increased with higher specific speed for the ESPs. This provides valuable information for system sizing, recognizing that more radial ESPs have their performance more affected by viscosity, while axial ESPs are less impaired.
- Regarding fluid heating, we observed that the temperature increase did not only depend on the ESP efficiency, but other operational parameters also influenced the fluid heating.

Nomenclature

BHP = brake horsepower, $mL^2\ t^{-3}$, watts
BHP_{disk} = disk friction loss, L, m
c_P = specific heat, $L^2t^{-2}T^{-1}$, J/kg·K
C_H = head correction factor, dimensionless
C_Q = flow rate correction factor, dimensionless
C_η = efficiency correction factor, dimensionless
D = impeller diameter, L, mm
f = friction factor, dimensionless
g = gravity acceleration, Lt^{-2}, m/s^2
h_f = friction loss, L, m
H = head, L, m
$\dot{m}_L$ = mass flow rate, mt^{-1}, kg/s
N = number of stages, dimensionless
N_S = specific speed, American units
P = pressure, $mL^{-1}t^{-2}$, Pa
P_h = hydraulic power, $mL^2\ t^{-3}$, watts
Q = volumetric flow rate, $L^3\ t^{-1}$, m^3/h
R^2 = coefficient of determination, dimensionless

Re_ω = rotational Reynolds number, dimensionless
T = temperature, T, °C
Γ = shaft torque, $mL^2 t^{-2}$, N·m
ΔP = pressure gain, $mL^{-1}t^{-2}$, Pa
ΔT = temperature increase, T, ºC
η = efficiency, dimensionless [%]
μ = dynamic viscosity, mLt, mPa·s
ν = kinematic viscosity, Lt^{-2}, mm^2/s
Π = power coefficient, dimensionless
ρ = density, mL^{-3}, kg/m^3
ϕ = flow rate coefficient, dimensionless
ψ = head coefficient, dimensionless
ω = rotational speed, nt^{-1}, rev/min
ω_S = specific speed, dimensionless

Acknowledgments

The authors thank PETROBRAS (Petróleo Brasileiro S/A), Brazil grant ID: 2017/00764-1, and ANP ("Commitment to Research and Development Investments") for providing financial support for this study. The authors also thank the Artificial Lift & Flow Assurance Research Group (ALFA) and the Center for Petroleum Studies (CEPETRO), all part of the University of Campinas (UNICAMP).

References

Amaral, G., Estevam, V., and Franca, F. A. 2009. On the Influence of Viscosity on ESP Performance. *SPE Prod & Oper* **24** (2): 303–311. SPE-110661-PA. https://doi.org/10.2118/110661-PA.

ANSI/HI 9.6.7, *Rotodynamic Pumps - Guideline for Effects of Liquid Viscosity on Performance*. 2021. Parsippany, New Jersey, USA: Hydraulic Institute.

API RP 11S2, *Recommended Practice for Electric Submersible Pump Testing*. 1997. Washington, D. C: American Petroleum Institute.

Banjar, H. M. 2018. *Experiments, CFD Simulation and Modeling of Oil Viscosity and Emulsion Effects on ESP Performance*. PhD Thesis, University of Tulsa, Tulsa, Oklahoma, USA.

Barrios, L., Scott, S., Rivera, R. et al. 2012. ESP Technology Maturation: Subsea Boosting System With High GOR and Viscous Fluids. Paper presented at the SPE Annual Technical Conference and Exhibition, San Antonio, Texas, USA, 8–10 October. SPE-159186-MS. https://doi.org/10.2118/159186-MS.

Biazussi, J. L. 2014. *A Drift-Flux Model for Gas-Liquid Flow in Electrical Submersible Pump Operating with Low Viscous Liquid*. PhD Thesis, University of Campinas, Brazil. https://doi.org/10.47749/T/UNICAMP.2014.937839.

Bulgarelli, N. A. V., Biazussi, J. L., Monte Verde, W. et al. 2021a. Experimental Investigation on the Performance of Electrical Submersible Pump (ESP) Operating with Unstable Water/Oil Emulsions. *J Pet Sci Eng* **197**: 107900. https://doi.org/10.1016/j.petrol.2020.107900.

Bulgarelli, N. A. V., Biazussi, J. L., Monte Verde, W. et al. 2021b. Relative Viscosity Model for Oil/Water Stable Emulsion Flow within Electrical Submersible Pumps. *Chem Eng Sci* **245**: 116827. https://doi.org/10.1016/j.ces.2021.116827.

Bulgarelli, N. A. V., Biazussi, J. L., Monte Verde, W. et al. 2022. A Novel Criterion Based on Slip Ratio to Assess the Flow Behavior of W/O Emulsions within Centrifugal Pumps. *Chem Eng Sci* **247**. https://doi.org/10.1016/j.ces.2021.117050.

Chapallaz, J. M., Eichenberger, P., and Fischer, G. 1992. *Manual on Pumps Used as Turbine*. Germany: MHPG Series.

Colodette, G., Pereira, C. A. G., Siqueira, C. A. M. et al. 2008. Flow Assurance and Artificial Lift Innovations for Jubarte Heavy Oil in Brazil. *SPE Proj Fac & Const* **3** (1): 1–8. SPE-117174-PA. https://doi.org/10.2118/117174-PA.

Costa, B. M. P., Oliveira, P. da S., and Roberto, M. A. R. 2013. Mudline ESP: Eletrical Submersible Pump Installed in a Subsea Skid. Paper presented at the Offshore Technology Conference, Houston, Texas, USA, 6–9 May. OTC-24201-MS. https://doi.org/10.4043/24201-MS.

Daugherty, R. L. 1926. *A Further Investigation of the Performance of Centrifugal Pumps When Pumping Oils*, Vol. 130, Vol. 130. Seneca Falls, New York, USA: Goulds Pumps, Inc., Bulletin.

Gülich, J. F. 1999a. Pumping Highly Viscous Fluids with Centrifugal Pumps - Part 1. *World Pumps* **395**: 30–34.

Gülich, J. F. 1999b. Pumping Highly Viscous Fluids with Centrifugal Pumps — Part 2. *World Pumps* **396**: 39–42. https://doi.org/10.1016/S0262-1762(00)87492-1.

Gülich, J. F. 2008. *Centrifugal Pumps*. Berlin, Heidelberg, Germany: Springer-Verlag.

Hole, G. 1994. Fluid Viscosity Effects on Centrifugal Pumps. *Pumps and Systems Magazine*.

Hydraulic Institute Standards. 1955. *Determination of Pump Performance When Handling Viscous Liquid*, 10th edition.

Ippen, A. T. 1946. The Influence of Viscosity on Centrifugal Pump Performance. *Trans ASME* **68**: 823–848.

Monte Verde, W. 2016. *Performance Modeling of ESP Pumps Performance Operating with Gas-Viscous Liquid Mixtures*. PhD Thesis, University of Campinas, Brazil. https://doi.org/10.47749/T/UNICAMP.2016.976346.

Monte Verde, W., Biazussi, J., Porcel, C. E. et al. 2021. Experimental Investigation of Pressure Drop in Failed Electrical Submersible Pump (ESP) under Liquid Single-Phase and Gas-Liquid Two-Phase Flow. *J Pet Sci Eng* **198**: 108127. https://doi.org/10.1016/j.petrol.2020.108127.

Monte Verde, W., Kindermann, E., Biazussi, J. L. et al. 2022. Performance Database of Electrical Submersible Pumps (ESPs) under Viscous Fluid Flow. Repositório de Dados de Pesquisa Da Unicamp, V1. https://doi.org/10.25824/redu/AQX7SK.

Morrison, G., Yin, W., Agarwal, R. et al. 2017. Evaluation of Effect of Viscosity on an Electrical Submersible Pump. Paper presented at the ASME 2017 Fluids Engineering Division Summer Meeting, Waikoloa, Hawaii, USA, 30 July–3 August. FEDSM2017-69157. https://doi.org/10.1115/FEDSM2017-69157.

Morrison, G., Yin, W., Agarwal, R. et al. 2018. Development of Modified Affinity Law for Centrifugal Pump to Predict the Effect of Viscosity. *J Energy Resour Technol* **140** (9). https://doi.org/10.1115/1.4039874.

Ofuchi, E. M., Cubas, J. M. C., Stel, H. et al. 2020. A New Model to Predict the Head Degradation of Centrifugal Pumps Handling Highly Viscous Flows. *J Pet Sci Eng* **187**: 106737. https://doi.org/10.1016/j.petrol.2019.106737.

Ofuchi, E. M., Stel, H., Vieira, T. S. et al. 2017. Study of the Effect of Viscosity on the Head and Flow Rate Degradation in Different Multistage Electric Submersible Pumps Using Dimensional Analysis. *J Pet Sci Eng* **156**: 442–450. https://doi.org/10.1016/j.petrol.2017.06.024.

Omar, K. A., Khaldi, A., and Ladouani, A. 2017. Prediction of Centrifugal Pump Performance Using Energy Loss Analysis. *Aust J Mech Eng* **15** (3): 210–221. https://doi.org/10.1080/14484846.2016.1252567.

Patil, A. and Morrison, G. 2019. Affinity Law Modified to Predict the Pump Head Performance for Different Viscosities Using the Morrison Number. *J Fluids Eng* **141** (2). https://doi.org/10.1115/1.4041066.

Perissinotto, R. M., Monte Verde, W., Castro, M. S. de. et al. 2019a. Experimental Investigation of Oil Drops Behavior in Dispersed Oil-Water Two-Phase Flow within a Centrifugal Pump Impeller. *Exp Therm Fluid Sci* **105**: 11–26. https://doi.org/10.1016/j.expthermflusci.2019.03.009.

Perissinotto, R. M., Monte Verde, W., Gallassi, M. et al. 2019b. Experimental and Numerical Study of Oil Drop Motion within an ESP Impeller. *J Pet Sci Eng* **175**: 881–895. https://doi.org/10.1016/j.petrol.2019.01.025.

Perissinotto, R. M., Monte Verde, W., Perles, C. E. et al. 2020. Experimental Analysis on the Behavior of Water Drops Dispersed in Oil within a Centrifugal Pump Impeller. *Exp Therm Fluid Sci* **112**: 109969. https://doi.org/10.1016/j.expthermflusci.2019.109969.

Porcel, C., Biazussi, J. L., Monte Verde, W. et al. 2022. Experimental Study on the Performance of Electrical Submersible Pump Operating with Ultraviscous Oil. *SPE J*. SPE-209221-PA(in press; posted 2 March 2022). https://doi.org/10.2118/209221-PA.

Rodrigues, R., Soares, R., Matos, J. S. de. et al. 2005. A New Approach For Subsea Boosting - Pumping Module On The Seabed. Paper presented at the Offshore Technology Conference, Houston, Texas, USA, 2–5 May. OTC-17398-MS. https://doi.org/10.4043/17398-MS.

Shakirov, A., Koropetsky, V., Alexeev, Y. et al. 2018. Ultra-High-Speed ESP Solution for High Sand Production – A Real Case Study. Paper presented at the SPE Middle East Artificial Lift Conference and Exhibition, Manama, Bahrain, 28–29 November. SPE-192472-MS. https://doi.org/10.2118/192472-MS.

Silva, J. M. S., Mattos, C., and Rittershaussen, J. 2000. First Installation of an Electrical Submersible Pump in Deep Water: RJS-477 Campos Basin (in Portuguese) Brazil. *Tech Bull* **43** (1): 69–83.

Solano, E. A. 2009. *Viscous Effects on the Performance of Electro Submersible Pumps (ESP's)*. MSc Thesis, University of Tulsa, Tulsa, Oklahoma, USA.

Stepanoff, A. J. 1949. How Centrifugals Perform When Pumping Viscous Oils, Power.

Stepanoff, A. J. 1957. *Centrifugal and Axial Flow Pumps: Theory, Design, and Application*, second edition. New York, New York, USA: John Wiley & Sons, Inc.

Sun, D. and Prado, M. G. 2006. Single-Phase Model for Electric Submersible Pump (ESP) Head Performance. *SPE J.* **11** (1): 80–88. SPE-80925-PA. https://doi.org/10.2118/80925-PA.

Takacs, G. 2009. *Electrical Submersible Pumps Manual*. Cambridge, Massachusetts, USA: Elsevier Inc. https://doi.org/10.1016/B978-1-85617-557-9.X0001-2.

Turzo, Z., Takacs, G., and Zsuga, J. A. 2000. Computerized Model for Viscosity Correction of Centrifugal Pump Performance Curves. Paper presented at the 47th Southwestern Petroleum Short Course, Texas, USA.

Van Esch, B. P. M. 1997. *Simulation of Three-Dimensional Unsteady Flow in Hydraulic Pumps*. Thesis, University of Twente, The Netherlands.

Zhang, J. 2017. *Experiments, CFD Simulation and Modeling of ESP Performance under Viscous Fluid Flow Conditions*. MSc Thesis, University of Tulsa, Tulsa, Oklahoma, USA.

Zhu, J., Banjar, H., Xia, Z. et al. 2016. CFD Simulation and Experimental Study of Oil Viscosity Effect on Multi-Stage Electrical Submersible Pump (ESP) Performance. *J Pet Sci Eng* **146**: 735–745. https://doi.org/10.1016/j.petrol.2016.07.033.

Zhu, J., Zhu, H., Cao, G. et al. 2019. A New Mechanistic Model to Predict Boosting Pressure of Electrical Submersible Pumps under High-Viscosity Fluid Flow with Validations by Experimental Data. *SPE J.* **25** (2): 744–758. SPE-194384-MS. https://doi.org/10.2118/194384-MS.